PERGAMON

International Journal of Solids and Structures 36 (1999) 4563–4586

INTERNATIONAL JOURNAL OF SOLIDS and STRUCTURES

Re-polarization of elastic waves at a frictional contact interface—II. Incidence of a P or SV wave

Yue-Sheng Wang[a,*], Gui-Lan Yu[b]

[a] *Institute of Engineering Mechanics, Northern Jiaotong University, Beijing 100044, People's Republic of China*
[b] *Department of Civil Engineering, Northern Jiaotong University, Beijing 100044, People's Republic of China*

Received 4 January 1998; in revised form 29 June 1998

Abstract

This is Part II of a two-part paper which analyses the re-polarization of elastic waves at a frictional contact interface between two solids. The re-polarization of SH waves was solved in Part I by the use of the Fourier analysis. Here, in Part II, we consider the re-polarization of P or SV waves. It is assumed that the two solids are pressed together and, at the same time, loaded by anti-plane and in-plane shearing traction. If the incident wave is sufficiently strong, localized separation and slip may take place at the interface. As a result, the incident in-plane wave is re-polarized at the interface so that the anti-plane waves (SH waves) are induced. Using the method similar to that of Part I and considering the boundary conditions involving separation and slip, we manage to reduce the problem to a set of algebraic equations coupled with simple integral equations. An iterative method is developed based on the solution to the perfectly bonded interface. The locations and sizes of the separation and slip zones, the interface traction, the slip velocities, the global sliding velocities and the energy dissipation and partition are displayed for the case of two identical materials. It is found that the separation zones and the gaps are independent of the induced waves.

1. Introduction

The reflection and refraction of elastic waves at an interface between two solids is a fundamental topic in many fields such as seismology, geophysics, earthquake engineering, non-destructive evaluation, etc. This problem is customarily treated on the basis that the interface is perfectly bonded. Such an interface can transmit both tensile and compressive traction without discontinuity in displacements. The associated problem is a linear one and has been studied extensively. An opposite case is the contact interface which cannot transmit tensile traction. If the waves are strong enough, the local slip and separation may take place at the interface. Examples of such situations

* Corresponding author. Fax: 00 86 10 6224 5826; e-mail: yswang@center.njtu.edu.cn

0020-7683/99/$ - see front matter
PII: S0020-7683(98)00208-X

may include the propagation of seismic waves through a pre-existing fault surface and the wave propagation in mechanical systems with bolted or press-fit connections. In Part I of this two-part paper (Wang et al., 1998), we gave a brief review of the previously published papers concerning the interaction of elastic waves with a contact interface. Among them, the works by Comninou and Dundurs (see the references listed in Part I) are most noticeable. It is noted that they treated the in-plane and anti-plane wave motion separately. However we argue that SH and P/SV waves may be coupled with each other at a frictional contact interface in some cases. A new and interesting phenomenon—the re-polarization of SH waves at a frictional contact interface was examined in Part I by the present authors. The induced in-plane waves and their coupling to SH waves were discussed. The results show that, although the induced waves carry a small amount of energy, its effects on local slip and interface traction cannot be neglected. Here in Part II, a similar approach will be used to deal with the re-polarization of P or SV waves. It is noted that an incident in-plane wave, if strong enough, may cause the localized separation of the interface, while an incident anti-plane wave can not. Therefore the present problem is more complex than that considered in Part I. The solution of the problem should be of interest to scientists working with laboratory and field seismic data or to those working with non-destructive evaluation.

2. Problem formulation

The problem considered in this paper is shown in Fig. 1. Two elastic half-spaces are forced together by the applied pressure p_0 and, at the same time, loaded by the in-plane shearing traction q_0 as well as the anti-plane shearing traction τ_0. The Couloumb frictional model is adopted along the interface with static and kinetic friction coefficients as f_s and f_k. An incident harmonic P or SV wave ($n = 0$) strikes the interface under the angle θ_0, and is reflected and refracted at the interface. If the incident wave is strong enough, the interface will separate and slip locally. Consequently, the applied anti-plane shearing traction τ_0 may lead to the anti-plane slip of the interface, and thus induces the SH waves in two component materials. The notation we follow is the same as that in Part I. The indices $n = 1, 2, 3, 4$, which may appear in suffix or affix positions are to distinguish between the reflected and refracted P and SV waves, and $n = 2', 4'$ to distinguish between the induced SH waves in the lower and upper half space. The displacements associated with the different waves are taken as the real part of the typical form

$$\mathbf{u}^{(n)} = C_n \mathbf{d}^{(n)} \exp(iy_n), \quad n = 0, 1, 2, 2', 3, 4, 4', \tag{1}$$

with

$$y_n = k_n[\mathbf{x} \cdot \mathbf{p}^{(n)} - c_n t], \tag{2}$$

where k_n is the corresponding wave number; $\mathbf{d}^{(n)}$ and $\mathbf{p}^{(n)}$ are, respectively, the unit vectors defining the directions of motion and propagation. For P-wave incidence, $c_0 = c_L$ and

$$\mathbf{d}^{(0)} = \mathbf{p}^{(0)} = (\sin\theta_0, \cos\theta_0, 0), \tag{3}$$

while for SV-wave incidence, $c_0 = c_T$ and

$$\mathbf{d}^{(0)} = (-\cos\theta_0, \sin\theta_0, 0), \quad \mathbf{p}^{(0)} = (\sin\theta_0, \cos\theta_0, 0). \tag{4}$$

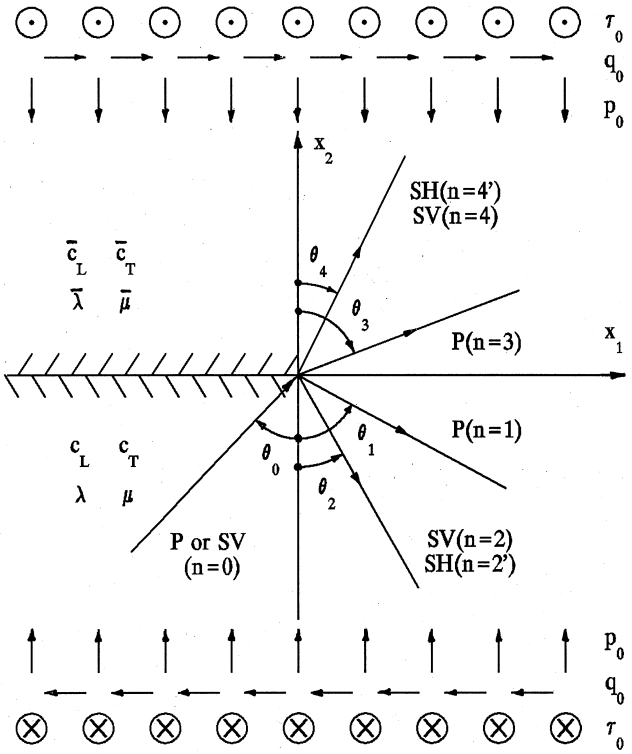

Fig. 1. Interaction of a P or SV wave with a frictional contact interface.

Other $\mathbf{d}^{(n)}$ and $\mathbf{p}^{(n)}$ ($n \neq 0$) may be found in the Appendix of Part I. The amplitude C_n is generally complex.

Snell's law which still holds for the unilateral interface (Comninou and Dundurs, 1979; Wang et al., 1998) leads to

$$\eta_0 = \eta_1 = \eta_2 = \eta_3 = \eta_4 \triangleq \eta^{\mathrm{PSV}}, \quad \eta_{2'} = \eta_{4'} \triangleq \eta^{\mathrm{SH}} \tag{5}$$

where $\eta_n = y_n|_{x_2 = 0}$. Since the SH waves are induced by the in-plane waves, it is reasonable to assert (Wang et al., 1998)

$$\eta^{\mathrm{PSV}} = \eta^{\mathrm{SH}} \triangleq \eta. \tag{6}$$

Then it follows from eqns (5) and (6) that $\theta_{2'} = \theta_2$, $\theta_{4'} = \theta_4$, and

$$\frac{\sin\theta_0}{c_0} = \frac{\sin\theta_1}{c_{\mathrm{L}}} = \frac{\sin\theta_2}{c_{\mathrm{T}}} = \frac{\sin\theta_3}{\bar{c}_{\mathrm{L}}} = \frac{\sin\theta_4}{\bar{c}_{\mathrm{T}}}, \tag{7}$$

$$k_0 c_0 = k_1 c_{\mathrm{L}} = k_2 c_{\mathrm{T}} = k_3 \bar{c}_{\mathrm{L}} = k_4 \bar{c}_{\mathrm{T}} = \omega. \tag{8}$$

The present analysis will be limited to the case of sub-critical angle incidence, that is, θ_0 should satisfy

$$\theta_0 < \theta_{cr} = \min\{\sin^{-1}(c_0/c_L), \sin^{-1}(c_0/\bar{c}_L)\}. \tag{9}$$

Because of the periodicity of the problem in η, only one representative interval, say $-\pi < \eta < \pi$, need to be considered. Denote the normal traction at the interface by $N(\eta)$, the in-plane and anti-plane shearing traction by $S_1(\eta)$ and $S_3(\eta)$, the gap by $g(\eta)$ and the relative slip velocities in x_1- and x_3-direction by $V_1(\eta)$ and $V_3(\eta)$. Then the boundary conditions may be written as

$$N(\eta) = S_1(\eta) = S_3(\eta) = 0 \tag{10}$$

$$g(\eta) > 0 \tag{11}$$

in the separation zones,

$$N(\eta) < 0, \quad S_1^2(\eta) + S_3^2(\eta) = [f_k N(\eta)]^2 \tag{12}$$

$$g(\eta) = 0, \quad \frac{V_1(\eta)}{S_1(\eta)} = \frac{V_3(\eta)}{S_3(\eta)}, \quad \text{sign}(V_j) = \text{sign}(S_j) \tag{13}$$

in the slip zones, and

$$N(\eta) < 0, \quad \sqrt{S_1^2(\eta) + S_3^2(\eta)} < f_s|N(\eta)| \tag{14}$$

$$g(\eta) = 0, V_1(\eta) = V_3(\eta) = 0 \tag{15}$$

in the stick zones. It is convenient in the subsequent analysis to replace the condition $g(\eta) = 0$ in eqns (13) and (15) with the weaker condition

$$V_2(\eta) = \dot{g}(\eta) = 0 \tag{16}$$

and to make special consideration ensuring that the gap indeed vanishes in the slip and stick zones. $V_2(\eta)$ is nothing but the opening velocity in the separation zones.

As in Part I, we construct the solution by adding the corrective solution $\{\bar{u}_i, \bar{\sigma}_{ij}\}$ to the results for the welded interface problem $\{u_i, \sigma_{ij}\}$. Then the interface traction, the opening velocity and the relative slip velocities can be expressed as

$$N(\eta) = -p_0 + [\sigma_{22}^{(0)} + \sigma_{22}^{(1)} + \sigma_{22}^{(2)} + \bar{\sigma}_{22}^{(1)} + \bar{\sigma}_{22}^{(2)}]_{x_2=0} = -p_0 + [\sigma_{22}^{(3)} + \sigma_{22}^{(4)} + \bar{\sigma}_{22}^{(3)} + \bar{\sigma}_{22}^{(4)}]_{x_2=0} \tag{17}$$

$$S_1(\eta) = q_0 + [\sigma_{12}^{(0)} + \sigma_{12}^{(1)} + \sigma_{12}^{(2)} + \bar{\sigma}_{12}^{(1)} + \bar{\sigma}_{12}^{(2)}]_{x_2=0} = q_0 + [\sigma_{12}^{(3)} + \sigma_{12}^{(4)} + \bar{\sigma}_{12}^{(3)} + \bar{\sigma}_{12}^{(4)}]_{x_2=0} \tag{18}$$

$$S_3(\eta) = \tau_0 + [\bar{\sigma}_{23}^{(2')}]_{x_2=0} = \tau_0 + [\bar{\sigma}_{23}^{(4')}]_{x_2=0} \tag{19}$$

$$V_2(\eta) = [\dot{\bar{u}}_2^{(3)} + \dot{\bar{u}}_2^{(4)} - \dot{\bar{u}}_2^{(1)} - \dot{\bar{u}}_2^{(2)}]_{x_2=0} \tag{20}$$

$$V_1(\eta) = [\dot{\bar{u}}_1^{(3)} + \dot{\bar{u}}_1^{(4)} - \dot{\bar{u}}_1^{(1)} - \dot{\bar{u}}_1^{(2)}]_{x_2=0} \tag{21}$$

$$V_3(\eta) = [\dot{\bar{u}}_3^{(4')} - \dot{\bar{u}}_3^{(2')}]_{x_2=0}. \tag{22}$$

The bilateral solution for the case of welded interface can be found in any book dealing with elastic waves, for instance, the book by Achenbach (1973), or in the paper by Comninou and Dundurs (1979). The normal and shearing traction transmitted by a perfectly bonded interface can be obtained by a straight forward calculation as

$$[\sigma_{22}]_{x_2=0} = [\sigma_{22}^{(0)} + \sigma_{22}^{(1)} + \sigma_{22}^{(2)}]_{x_2=0} = [\sigma_{22}^{(3)} + \sigma_{22}^{(4)}]_{x_2=0} = -Re\{iA_0 \exp(i\eta)\}, \tag{23}$$

$$[\sigma_{21}]_{x_2=0} = [\sigma_{21}^{(0)} + \sigma_{21}^{(1)} + \sigma_{21}^{(2)}]_{x_2=0} = [\sigma_{21}^{(3)} + \sigma_{21}^{(4)}]_{x_2=0} = -Re\{iB_0 \exp(i\eta)\} \tag{24}$$

where A_0 and B_0 are quite complicated and not readily open to interpretation. Comninou and Dundurs presented the expressions for P-wave incidence. They especially gave the results for the identical materials (see Comninou and Dundurs, 1979, eqns (3.11)–(3.14)).

3. Corrective solution

For the harmonic incident P or SV wave, the corrective solution may be expressed as the following Fourier series containing all higher frequencies:

$$\bar{\mathbf{u}}^{(n)} = \{U_1 t, 0, U_3 t\} + Re\left[\mathbf{d}^{(n)} \sum_{m=1}^{\infty} F_m^{(n)} \exp(imy_n)\right], \quad n = 1, 2(2'), 3, 4(4'), \tag{25}$$

where U_1 and U_3 represent, respectively, the global sliding velocities in x_1- and x_3-direction due to the in-plane and anti-plane shearing traction. $F_m^{(n)}$ is a coefficient to be determined and may be written as $F_m^{(n)} = D_m^{(n)} + iE_m^{(n)}$ with $D_m^{(n)}$ and $E_m^{(n)}$ being real.

The requirement that the normal and shearing traction be continuous across the interface allows us to write (see Part I for details, Wang et al., 1988)

$$N(\eta) = -p_0 + A_0 \sin\eta + \mu \sum_{m=1}^{\infty} m(M_m \sin m\eta + L_m \cos m\eta) \tag{26}$$

$$S_1(\eta) = q_0 + B_0 \sin\eta + \mu \sum_{m=1}^{\infty} m(I_m \sin m\eta + J_m \cos m\eta) \tag{27}$$

$$S_3(\eta) = \tau_0 + \mu k_2 \cos\theta_2 \sum_{m=1}^{\infty} m(D_m^{(2')} \sin m\eta + E_m^{(2')} \cos m\eta) \tag{28}$$

$$V_2(\eta) = c_L \sum_{m=1}^{\infty} m[(\lambda_1 I_m - \lambda_2 M_m) \sin m\eta + (\lambda_1 J_m - \lambda_2 L_m) \cos m\eta] \tag{29}$$

$$V_1(\eta) = U_1 - c_L \sum_{m=1}^{\infty} m[(\lambda_3 I_m + \lambda_1 M_m) \sin m\eta + (\lambda_3 J_m + \lambda_1 L_m) \cos m\eta] \tag{30}$$

$$V_3(\eta) = U_3 - k_2 c_T b \sum_{m=1}^{\infty} m(D_m^{(2')} \sin m\eta + E_m^{(2')} \cos m\eta), \tag{31}$$

where

$$b = 1 + \frac{\gamma_T \cos\theta_2}{\Gamma \cos\theta_4}$$

$$\{I_m, J_m\} = k_1 \sin 2\theta_1 \{D_m^{(1)}, E_m^{(1)}\} + k_2 \cos 2\theta_2 \{D_m^{(2)}, E_m^{(2)}\}$$

$$\{M_m, L_m\} = -k_2 \kappa \cos 2\theta_2 \{D_m^{(1)}, E_m^{(1)}\} + k_2 \sin 2\theta_2 \{D_m^{(2)}, E_m^{(2)}\},$$

and Γ, γ_T, κ, λ_j $(j=1,2,3)$ are given in Comninou and Dundurs (1979). It follows from eqns (29)–(31) that

$$\{U_1, 0, U_3\} = \frac{1}{2\pi}\int_{-\pi}^{\pi} \{V_1(\xi), V_2(\xi), V_3(\xi)\}\,\mathrm{d}\xi \tag{32}$$

$$\{\lambda_3 I_m + \lambda_1 M_m, \lambda_3 J_m + \lambda_1 L_m\} = \frac{-1}{\pi c_L m}\int_{-\pi}^{\pi} V_1(\xi)\,\{\sin m\xi, \cos m\xi\}\,\mathrm{d}\xi \tag{33}$$

$$\{\lambda_1 I_m - \lambda_2 M_m, \lambda_1 J_m - \lambda_2 L_m\} = \frac{-1}{\pi c_L m}\int_{-\pi}^{\pi} V_2(\xi)\{\sin m\xi, \cos m\xi\}\,\mathrm{d}\xi \tag{34}$$

$$\{D_m^{(2')}, E_m^{(2')}\} = \frac{-1}{\pi k_2 c_T b m}\int_{-\pi}^{\pi} V_3(\xi)\{\sin m\xi, \cos m\xi\}\,\mathrm{d}\xi. \tag{35}$$

Then the interface traction $N(\eta)$, $S_1(\eta)$ and $S_3(\eta)$ may be expressed as

$$N(\eta) = -p_0 + A_0 \sin\eta + A_0\left\{\frac{\lambda_1}{\lambda_2}\beta^{-1}[\bar{U}_1 - \bar{V}_1(\eta)] - \frac{\lambda_3}{\lambda_2}\bar{V}_2(\eta)\right\} \tag{36}$$

$$S_1(\eta) = q_0 + B_0 \sin\eta + B_0\left\{[\bar{U}_1 - \bar{V}_1(\eta)] + \frac{\lambda_1}{\lambda_2}\beta\bar{V}_2(\eta)\right\} \tag{37}$$

$$S_3(\eta) = \tau_0 + \alpha B_0[\bar{U}_3 - \bar{V}_3(\eta)], \tag{38}$$

where we have denoted $\alpha = a\kappa b^{-1}\cos\theta_2$, $\beta = A_0/B_0$ and

$$\{\bar{V}_1, \bar{V}_2, \bar{V}_3, \bar{U}_1, \bar{U}_3\} = \frac{\mu B_0^{-1}}{c_L a}\{V_1, \beta^{-1}V_2, V_3, U_1, U_3\}, \tag{39}$$

with $a = (\lambda_1^2/\lambda_2 + \lambda_3)$.

Considering the boundary conditions in separation zones, eqn (10), we have

$$\bar{V}_2(\eta) = -a^{-1}(\lambda_2 p_0/A_0 + \lambda_1\beta^{-1}q_0/B_0) + a^{-1}(\lambda_2 - \lambda_1\beta^{-1})\sin\eta \tag{40}$$

$$\bar{U}_1 - \bar{V}_1(\eta) = a^{-1}(\lambda_1\beta p_0/A_0 - \lambda_3 q_0/B_0) - a^{-1}(\lambda_3 + \lambda_1\beta)\sin\eta \tag{41}$$

$$\bar{U}_3 - \bar{V}_3(\eta) = -\alpha^{-1}\tau_0/B_0. \tag{42}$$

The gap can be calculated by

$$g(\eta) = -\frac{aA_0}{\mu k_1}\int \bar{V}_2(\eta)\,\mathrm{d}\eta = \frac{A_0}{\mu k_1}[(\lambda_2 p_0/A_0 + \lambda_1\beta^{-1}q_0/B_0)\eta + (\lambda_2 - \lambda_1\beta^{-1})\cos\eta - L], \tag{43}$$

where L is a constant which can be determined by the fact that the gap vanishes at both ends of the separation zone. If we denote the separation zone as (δ_1, δ_2), L is given by

$$L = (\lambda_2 p_0/A_0 + \lambda_1\beta^{-1} q_0/B_0)\delta_1 + (\lambda_2 - \lambda_1\beta^{-1})\cos\delta_1$$
$$= (\lambda_2 p_0/A_0 + \lambda_1\beta^{-1} q_0/B_0)\delta_2 + (\lambda_2 - \lambda_1\beta^{-1})\cos\delta_2. \tag{44}$$

It is noted that the gap given by eqn (43) is independent of the induced anti-plane waves and is exactly the same as that for $\tau_0 = 0$ (see eqn (5.1) of Comninou and Dundurs, 1979). Furthermore, one can verify that the interface normal traction $N(\eta)$ in the present case is of the same form as that of Comninou and Dundurs (1979) although the values of $\bar{U}_1$ and $\bar{V}_1(\eta)$ in these two situations are different. Therefore we believe that the separation zone (δ_1, δ_2) may be determined in the way developed by Comninou and Dundurs (1977, 1979). Make A_0 positive by adjusting the sign of C_0. Comninou and Dundurs found that, when

$$\lambda_2 p_0/A_0 + \lambda_1\beta^{-1} q_0/B_0 > 0, \tag{45}$$

the gap opens smoothly at the leading edge, δ_2, which is determined by

$$\sin\delta_2 = \frac{\lambda_2 p_0/A_0 + \lambda_1\beta^{-1} q_0/B_0}{\lambda_2 - \lambda_1\beta^{-1}}, \quad \delta_2 > \frac{\pi}{2}. \tag{46}$$

At the trailing edge, δ_1, the gap closes discontinuously. δ_1 can be obtained from eqn (44). If eqn (45) is violated, the behavior of the two edges interchange. In this case,

$$\sin\delta_1 = \frac{\lambda_2 p_0/A_0 + \lambda_1\beta^{-1} q_0/B_0}{\lambda_2 - \lambda_1\beta^{-1}}, \quad \delta_1 < \frac{\pi}{2}, \tag{47}$$

and δ_2 can be calculated from eqn (44).

We anticipate that the above results given by Comninou and Dundurs (1979) for $\tau_0 = 0$ are valid in the presence of τ_0. Of course, the real separation zones should be determined to ensure $N(\eta) < 0$ in slip and stick zones and $g(\eta) > 0$ in separation zones. An example will be given afterwards to demonstrate the procedure determining the separation of the interface.

Next we consider the solution in the slip zones. Substitution of eqns (36)–(38) into the boundary conditions (12) and (13) yields

$$\{q_0/B_0 + \sin\eta + [\bar{U}_1 - \bar{V}_1(\eta)]\}^2 + \{\tau_0/B_0 + \alpha[\bar{U}_3 - \bar{V}_3(\eta)]\}^2$$
$$= (f_k\beta)^2\left\{-p_0/A_0 + \sin\eta + \frac{\lambda_1}{\lambda_2}\beta^{-1}[\bar{U}_1 - \bar{V}_1(\eta)]\right\}^2 \tag{48}$$

$$\bar{V}_1(\eta)/\{q_0/B_0 + \sin\eta + [\bar{U}_1 - \bar{V}_1(\eta)]\} = \bar{V}_3(\eta)/\{\tau_0/B_0 + \alpha[\bar{U}_3 - \bar{V}_3(\eta)]\}. \tag{49}$$

In the stick zones, we have

$$\bar{V}_1(\eta) = \bar{V}_3(\eta) = 0. \tag{50}$$

Moreover eqn (32) yields

$$\{\bar{U}_1, \bar{U}_3\} = \frac{1}{2\pi}\int_{-\pi}^{\pi}\{\bar{V}_1(\eta), \bar{V}_3(\eta)\}\,\mathrm{d}\eta. \tag{51}$$

The remaining task is to determine the slip zones. To this end, we follow the procedure described in Part I (Wang et al., 1988). Suppose (α_j, β_j) is a slip zone. The two edges satisfy

$$(\tau_0/B_0+\alpha\bar{U}_3)^2+(q_0/B_0+\sin\beta_j+\bar{U}_1)^2=(f_s\beta)^2\left(-p_0/A_0+\sin\beta_j+\frac{\lambda_1}{\lambda_2}\beta^{-1}\bar{U}_1\right)^2 \tag{52}$$

$$(\tau_0/B_0+\alpha\bar{U}_3)^2+(q_0/B_0+\sin\alpha_j+\bar{U}_1)^2=(f_k\beta)^2\left(-p_0/A_0+\sin\alpha_j+\frac{\lambda_1}{\lambda_2}\beta^{-1}\bar{U}_1\right)^2. \tag{53}$$

The extent and location of the real slip zones should be determined by consideration of inequality in eqn (14).

It should be noted that eqns (52) and (53) are coupled with eqns (41), (42) and (48)–(51). It is almost impossible to obtain the analytic solution to the problem. Thus, to get numerical results, the iterative method similar to that used in Part I will be used. Numerical computations for identical materials will be performed in detail afterwards. Before further discussion of the problem, it is worthwhile to examine some limiting situations.

(i) $A_0=0$

In this limiting case, the incident wave does not generate normal traction at the welded interface. Then eqn (36) reduces to

$$N(\eta)=-p_0+B_0\frac{\lambda_1}{\lambda_2}[\bar{U}_1-\bar{V}_1(\eta)]. \tag{54}$$

Consequently, the interface does not separate. Only slip zones may take place, where the following relations should be satisfied

$$\{q_0/B_0+\sin\eta+[\bar{U}_1-\bar{V}_1(\eta)]\}^2+\{\tau_0/B_0+\alpha[\bar{U}_3-\bar{V}_3(\eta)]\}^2 = f_k^2\left\{-p_0/B_0+\frac{\lambda_1}{\lambda_2}[\bar{U}_1-\bar{V}_1(\eta)]\right\}^2 \tag{55}$$

$$\bar{V}_1(\eta)/\{q_0/B_0+\sin\eta+[\bar{U}_1-\bar{V}_1(\eta)]=\bar{V}_3(\eta)/\{\tau_0/B_0+\alpha[\bar{U}_3-\bar{V}_3(\eta)]\}. \tag{56}$$

The above two equations are, respectively, similar to eqns (43) and (44) in Part I (Wang et al., 1998) and may be solved analogously.

(ii) $B_0=0$

Introducing the nondimensionalized quantities

$$\{\tilde{V}_1,\tilde{V}_3,\tilde{U}_1,\tilde{U}_3\}=\frac{\mu A_0^{-1}}{c_L a}\{V_1,V_3,U_1,U_3\}, \tag{57}$$

and following the previous analysis, one obtains, in the separation zones,

$$\bar{V}_2(\eta)=-a^{-1}(\lambda_2 p_0/A_0+\lambda_1 q_0/A_0)+a^{-1}\lambda_2\sin\eta \tag{58}$$

$$\bar{U}_1-\bar{V}_1(\eta)=a^{-1}(\lambda_1 p_0/A_0-\lambda_3 q_0/A_0)-a^{-1}\lambda_1\sin\eta \tag{59}$$

$$\tilde{U}_3 - \tilde{V}_3(\eta) = -\alpha^{-1}\tau_0/A_0. \tag{60}$$

The separation zones and the gaps can be determined as before. In the slip zones, we have

$$\{q_0/A_0 + [\tilde{U}_1 - \tilde{V}_1(\eta)]\}^2 + \{\tau_0/A_0 + \alpha[\tilde{U}_3 - \tilde{V}_3(\eta)]\}^2 = f_k^2\left\{-p_0/A_0 + \sin\eta + \frac{\lambda_1}{\lambda_2}[\tilde{U}_1 - \tilde{V}_1(\eta)]\right\}^2 \tag{61}$$

$$\tilde{V}_1(\eta)/\{q_0/A_0 + [\tilde{U}_1 - \tilde{V}_1(\eta)]\} = \tilde{V}_3(\eta)/\{\tau_0/A_0 + \alpha[\tilde{U}_3 - \tilde{V}_3(\eta)]\}. \tag{62}$$

(iii) $f_k = f_s = 0$

The interface cannot undergo shearing traction in this case. Therefore we have to set $q_0 = \tau_0 = 0$. Then the present problem reduces to the problem of interaction between in-plane waves and a smoothly contact interface (Comninou and Dundurs, 1977).

(iv) $f_k \to \infty$

It is clear that the local slip cannot take place in this case. Thus when

$$\left|\frac{\lambda_2 p_0/A_0 + \lambda_1\beta^{-1}q_0/B_0}{\lambda_2 - \lambda_1\beta^{-1}}\right| \geqslant 1, \tag{63}$$

the interface is perfectly in contact, otherwise the solids will separate locally and slide in a creeping manner without local slip. The creeping velocities may be calculated from eqns (41), (42) and (51) as

$$\bar{U}_1 = \frac{a^{-1}(\delta_1 - \delta_2)(\lambda_1\beta p_0/A_0 - \lambda_3 q_0/B_0) + a^{-1}(\cos\delta_1 - \cos\delta_2)(\lambda_3 + \lambda_1\beta)}{2\pi - (\delta_2 - \delta_1)} \tag{64}$$

$$\bar{U}_3 = \frac{(\delta_2 - \delta_1)\alpha^{-1}\tau_0/B_0}{2\pi - (\delta_2 - \delta_1)}. \tag{65}$$

4. Energy partition and dissipation

We examine the power averaged over a wave length or a period of the incident wave, which is inputted to, extracted from and dissipated at a thin slice of material containing the interface.

The power input of the applied in-plane and anti-plane shearing traction is given by eqn (54) in Part I (Wang et al., 1998), whereas the input of the incident wave is

$$P_0 = -\frac{1}{2\pi}\int_{-\pi}^{\pi}[\sigma_{12}^{(0)}\dot{u}_1^{(0)} + \sigma_{22}^{(0)}\dot{u}_2^{(0)}]\,\mathrm{d}\eta. \tag{66}$$

For P-wave incidence,

$$P_0 = \tfrac{1}{2}(\lambda + 2\mu)C_0^2 k_L^2 c_L \cos\theta_0, \tag{67}$$

and for SV-wave incidence,

$$P_0 = \tfrac{1}{2}\mu C_0^2 k_T^2 c_T \cos\theta_0. \tag{68}$$

The power extracted from the slice by the induced reflected and refracted SH waves is

$$P_1^{SH} = \frac{1}{2\pi}\int_{-\pi}^{\pi} \bar{\sigma}_{23}^{(2')}\dot{\bar{u}}_3^{(2')}\,d\eta, \quad P_2^{SH} = -\frac{1}{2\pi}\int_{-\pi}^{\pi} \bar{\sigma}_{23}^{(4')}\dot{\bar{u}}_3^{(4')}\,d\eta, \tag{69}$$

and that of the reflected and refracted in-plane waves (P and SV waves) is given by

$$P_1^{PSV} = \frac{1}{2\pi}\int_{-\pi}^{\pi} [\sigma_{22}^{(1)}+\sigma_{22}^{(2)}+\bar{\sigma}_{22}^{(1)}+\bar{\sigma}_{22}^{(2)}][\dot{u}_2^{(1)}+\dot{u}_2^{(2)}+\dot{\bar{u}}_2^{(1)}+\dot{\bar{u}}_2^{(2)}]\,d\eta$$
$$+\frac{1}{2\pi}\int_{-\pi}^{\pi} [\delta_{12}^{(1)}+\sigma_{12}^{(2)}+\bar{\sigma}_{12}^{(1)}+\bar{\sigma}_{12}^{(2)}][\dot{u}_1^{(1)}+\dot{u}_1^{(2)}+\dot{\bar{u}}_1^{(1)}+\dot{\bar{u}}_1^{(2)}]\,d\eta \tag{70}$$

$$P_2^{PSV} = -\frac{1}{2\pi}\int_{-\pi}^{\pi} [\sigma_{22}^{(3)}+\sigma_{22}^{(4)}+\sigma_{22}^{(3)}+\bar{\sigma}_{22}^{(4)}][\dot{u}_2^{(3)}+\dot{u}_2^{(4)}+\dot{\bar{u}}_2^{(3)}+\dot{\bar{u}}_2^{(4)}]\,d\eta$$
$$-\frac{1}{2\pi}\int_{-\pi}^{\pi} [\sigma_{12}^{(3)}+\sigma_{12}^{(4)}+\bar{\sigma}_{12}^{(3)}+\bar{\sigma}_{12}^{(4)}][\dot{u}_1^{(3)}+\dot{u}_1^{(4)}+\dot{\bar{u}}_1^{(3)}+\dot{\bar{u}}_1^{(4)}]\,d\eta. \tag{71}$$

The power dissipated by friction at the interface can be divided into two parts. One is due to slip in the x_1-direction caused by the interface shearing traction $S_1(\eta)$, another is due to slip in the x_3-direction caused by $S_3(\eta)$. They can be calculated by eqns (60) and (61) in Part I. The energy conservation relation as eqn (62) in Part I still holds here.

5. Numerical example and discussion

As in Part I, we will carry out computations for identical materials to give explicit exploration to the re-polarization of elastic waves. For simplicity, we neglect the in-plane shearing traction and the kinematic locking, i.e. $q_0 = 0$ and $f_k = f_s = f$.

We first consider the solution in the separation zones. The interface normal traction and the gap in this case may be written as

$$N(\eta)/A_0 = -p_0/A_0 + \sin\eta - \frac{\lambda_3}{\lambda_2}\bar{V}_2(\eta) \tag{72}$$

$$g(\eta) = \frac{\lambda_2 A_0}{\mu k_1}\bar{g}(\eta) = \frac{\lambda_2 A_0}{\mu k_1}[p_0/A_0\eta + \cos\eta - \bar{L}], \tag{73}$$

where

$$\bar{L} = p_0/A_0\delta_1 + \cos\delta_1 = p_0/A_0\delta_2 + \cos\delta_2. \tag{74}$$

It is seen that the normal traction $N(\eta)$ in the slip and stick zones is identical to that for a welded

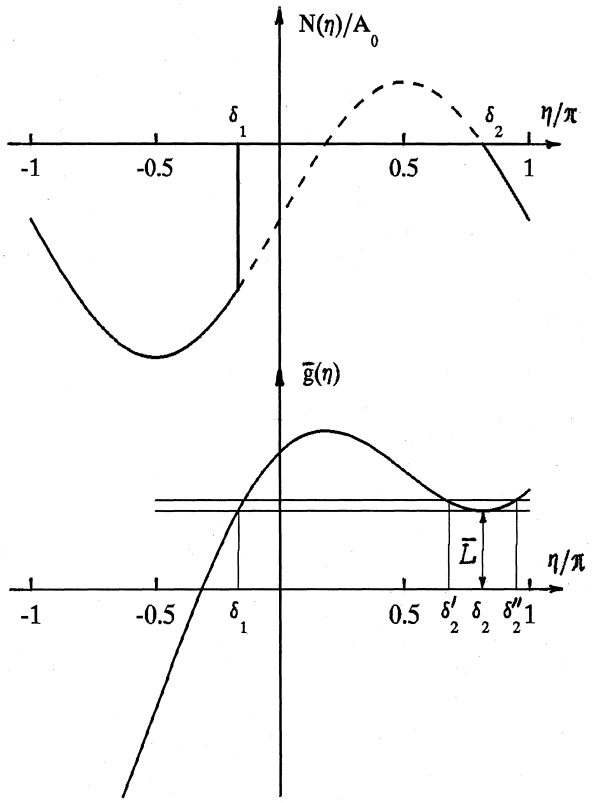

Fig. 2. Sketch map of $N(\eta)/A_0$ and $\tilde{g}(\eta)$.

interface. The sketch maps of $N(\eta)/A_0$ and $\tilde{g}(\eta)$ are depicted in Fig. 2 where (δ_1, δ_2) represents a separation zone. The leading edge δ_2 is given by

$$\delta_2 = \pi - \arcsin(p_0/A_0), \tag{75}$$

and the trailing edge δ_1 may be obtained from eqn (74). It can be easily verified that the conditions, $g(\eta) > 0$ for $\eta \in (\delta_1, \delta_2)$ and $N(\eta) < 0$ for $\eta \notin (\delta_1, \delta_2)$, are all satisfied. If we locate the leading edge to the left of δ_2, say δ_2' in Fig. 2, the normal traction $N(\eta) > 0$ in (δ_2', δ_2). On the other hand, if one locates the leading edge to the right of δ_2, as indicated by δ_2'' in Fig. 2, the gap $g(\eta) < 0$ in (δ_2, δ_2''). That is to say, the interval (δ_1, δ_2) is the only one separation zone that really exists in one representative period. It is noted that the separation zone, the gap and the interface normal traction depend upon only one parameter, p_0/A_0. When $p_0/A_0 > 1$, the solids cannot separate. The above result is identical to that for the case of $\tau_0 = 0$ (the case of no re-polarization involved, see Comninou and Dundurs, 1979), and also to that for a smoothly contact interface (Comninou and Dundurs, 1977). The velocities $\bar{V}_1(\eta)$ and $\bar{V}_3(\eta)$ in the separation zone are given by

$$\bar{V}_1(\eta) = \bar{U}_1 \sin\eta, \quad \bar{V}_3(\eta) = \bar{U}_3 + \alpha^{-1}\tau_0/B_0, \quad \eta \in (\delta_1, \delta_2) \tag{76}$$

where $\bar{U}_1$ and $\bar{U}_3$ are unknown and will be determined afterwards.

Now we turn to the slip zones. The interface shearing traction may be written as

$$S_1(\eta)/B_0 = \sin\eta + [\bar{U}_1 - \bar{V}_1(\eta)] \tag{77}$$

$$S_3(\eta)/B_0 = \tau_0/B_0 + \alpha[\bar{U}_3 - \bar{V}_3(\eta)]. \tag{78}$$

From eqns (52) and (53), we have the following relations that the edges of the slip zone should satisfy:

$$\sin\beta_j = \sin\alpha_j = \frac{-\bar{U}_1 - (f\beta)^2 p_0/A_0 \pm \sqrt{(f\beta)^2(\bar{U}_1 + p_0/A_0)^2 - [1-(f\beta)^2](\alpha\bar{U}_3 + \tau_0/B_0)^2}}{1-(f\beta)^2} \triangleq \Theta^{\pm} \tag{79}$$

for $f\beta \neq 1$, and

$$\sin\beta_j = \sin\alpha_j = \frac{1}{2}\frac{(p_0/A_0)^2 - \bar{U}_1^2 - (\tau_0/B_0 + \alpha\bar{U}_3)^2}{\bar{U}_1 + p_0/A_0} \triangleq \Theta \tag{80}$$

for $f\beta = 1$. To determine the number of the slip zones and the values of (α_j, β_j), it is necessary to anticipate the possible arrangements of the separation, slip and stick zones. We first consider the case without separation. One may note that the value of $N(\eta)$ reaches the minimum at $\eta = \pi/2$ and the maximum at $\eta = -\pi/2$, while the interface shearing traction $\sqrt{S_1^2(\eta) + S_3^2(\eta)}$ reaches the peak values with different directions at $\eta = \pm\pi/2$. Therefore, if the shearing traction is sufficiently strong, local slip will take place near $\eta = \pi/2$. Denote this slip zone as (α_2, β_2), see Fig. 3a. If the friction coefficient f is small enough and the pressure is not too strong, a local slip may occur near $\eta = -\pi/2$. This slip zone is denoted by (α_1, β_1) as shown in Fig. 3b. The slip zone (α_2, β_2) may grow

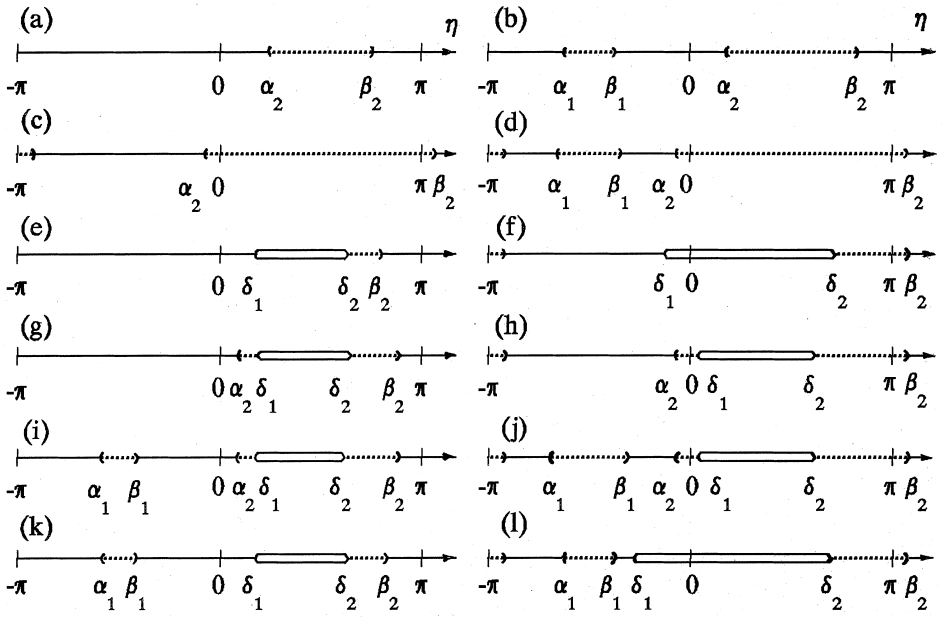

Fig. 3. Possible arrangement of the separation, slip and stick zones.

beyond $(0, \pi)$, as demonstrated in Fig. 3c, d. Next we discuss the case in presence of separation. It is seen from eqn (72) that $N(\delta_2) = 0$, but that the shearing traction does not necessarily vanish at $\eta = \delta_2$. Consequently, there must be a slip zone ahead of the separation zone as illustrated in Fig. 3e. This slip zone is denoted by (δ_2, β_2) where $\delta_2 < \pi$ and β_2 may locate beyond π (see Fig. 3f). However, there is not necessarily a slip zone connecting with the trailing edge of the separation zone. If there is, we denote it by (α_2, δ_1), as in Fig. 3g, h. As in the case without separation, another slip zone (α_1, β_1), may exist near $\eta = -\pi/2$, see Fig. 3i, j, k, l. This slip zone will connect with the separation zone if δ_1 reaches β_1. If the separation zone is so big that the trailing edge exceeds α_1, there is no slip zone behind the separation zone.

Based on the above analysis, eqn (79) yields

$$\alpha_2 = \pi - \beta_2 = \arcsin \Theta^+, f\beta \neq 1 \tag{81}$$

$$\beta_1 = -\pi - \alpha_1 = \arcsin \Theta^-, f\beta \neq 1 \tag{82}$$

with restriction of $\beta_1 < \alpha_2$. When $\delta_1 \leqslant \alpha_2$, the slip zone, (α_2, δ_1), behind the separation zone disappears. When $\delta_1 \leqslant \alpha_1$, both slip zones, (α_1, β_1) and (α_2, δ_1), disappear. If δ_1 falls between β_1 and α_2, (α_1, δ_1) is a slip zone. For $f\beta = 1$, eqn (80) gives

$$\alpha_2 = \pi - \beta_2 = \arcsin \Theta. \tag{83}$$

That is, the slip zone (α_1, β_1) does not exist in this situation. The above three equations cannot yield proper real values in some cases. These special situations include:

(i) When $\Theta^+ > 1$ (or $\Theta > 1$), i.e. when

$$p_0/A_0 > 1 + |f\beta|^{-1} \sqrt{1 + (\tau_0/B_0)^2} > 1, \tag{84}$$

there is no slip zone and, of course, no separation zone. The interface is welded.

(ii) When $\Theta^+ \leqslant 1$ (or $\Theta \leqslant 1$), the stick zones disappear. Then the whole interface is in slipping with possible separation zones.

(iii) When $\Theta^- \leqslant -1$, the slip zone, (α_1, β_1), disappears.

(iv) When the radicand in $\Theta^\pm$ is equal to zero, we have $\Theta^+ = \Theta^-$, that is, $\alpha_2 = \beta_1$. This means that the two slip zones are just connected, and that there is no stick zone on the interface. When the radicand is negative, eqns (81) and (82) cannot yield correct solutions any more, and the whole interface is in slipping without separation.

After determining the slip zones, we calculate the velocities therein. Equation (49) gives

$$\bar{V}_3(\eta) = \frac{\tau_0/B_0 + \alpha \bar{U}_3}{\sin \eta + \bar{U}_1 + (\alpha - 1)\bar{V}_1(\eta)} \bar{V}_1(\eta), \tag{85}$$

which when substituted into eqn (48) yields a quartic equation

$$\bar{V}_1^4(\eta) + \bar{b}\bar{V}_1^3(\eta) + \bar{c}\bar{V}_1^2(\eta) + \bar{d}\bar{V}_1(\eta) + \bar{e} = 0, \tag{86}$$

with

$$\bar{b} = 2(2 - \alpha)(\sin \eta + \bar{U}_1)/(\alpha - 1)$$

$$\bar{c} = [(\alpha^2 - 6\alpha + 6)(\sin \eta + \bar{U}_1)^2$$

$$-(f\beta)^2(\alpha-1)^2(-p_0/A_0+\sin\eta)^2+(\tau_0/A_0+\alpha\bar{U}_3)^2]/(\alpha-1)^2$$

$$\bar{d}=2(\sin\eta+\bar{U}_1)[(\alpha-2)(\sin\eta+\bar{U}_1)^2$$

$$-(f\beta)^2(\alpha-1)(-p_0/A_0+\sin\eta)^2-(\tau_0/B_0+\alpha\bar{U}_3)^2]/(\alpha-1)^2$$

$$\bar{e}=(\sin\eta+\bar{U}_1)^2[(\sin\eta+\bar{U}_1)^2-(f\beta)^2(-p_0/A_0+\sin\eta)^2+(\tau_0/B_0+\alpha\bar{U}_3)^2]/(\alpha-1)^2.$$

Equation (85) can be solved analytically by using Ferrari's method (Kern and Kern, 1974). Its four roots are exactly the same as those of the following two quadratic equations

$$\bar{V}_1^2(\eta)+\tilde{b}^{\pm}\bar{V}_1(\eta)+\tilde{c}^{\pm}=0, \tag{87}$$

where

$$\tilde{b}^{\pm}=\tfrac{1}{2}(\bar{b}\pm\sqrt{8y+\bar{b}^2-4\bar{c}}),\quad \tilde{c}^{\pm}=y\pm\frac{\bar{b}y-\bar{d}}{\sqrt{8y+\bar{b}^2-4\bar{c}}}$$

and y is any real one of the three roots of the cubic equation

$$8y^3-4\bar{c}y^2+(2\bar{b}\bar{d}-8\bar{e})y+\bar{e}(4\bar{c}-\bar{b}^2)-\bar{d}^2=0, \tag{88}$$

which can be solved analytically by using Cardano's method (Kern and Kern, 1974). For the case of $\alpha=1$ eqn (85) reduces to a quadratic equation of which the two roots may be found easily. Among the four or two roots of eqn (85) we should choose the real one which satisfies the condition $\bar{V}_1(\alpha_j)=\bar{V}_3(\beta_j)=0$.

Now we can carry out the computation based on the above equations by the iterative procedure described in Part I (Wang et al., 1998). The convergence was examined in that paper. The computation accuracy is kept at the level of 0.1%.

It can be seen that the solution of the problem depends on the four parameters: τ_0/B_0, p_0/A_0, $f\beta$ and α, where $\alpha(\geqslant 1)$ involves the effects of Poisson ratio v and the incident angle θ_0; and $f\beta$ is a parameter determining the difficulty of interface slip. In the following computation, the Poisson ratio v is taken to be 0.25. There is no critical angle for P-wave incidence. The critical incident angle for SV-wave incidence is $\theta_{cr}=\sin^{-1}(1/\kappa)=35.264^\circ$. In the present paper we only consider P-wave incidence.

Figure 4 illustrates the curves determining the extent and location of slip and separation zones for given p_0/A_0 and some selected values of τ_0/B_0 with $f\beta=0.2$ and $\theta_0=30^\circ$. The dotted line determines the separation zone which is independent of τ_0/B_0, $f\beta$ and α. The dashed line gives the slip zone for $\tau_0=0$, the case considered by Comninou and Dundurs (1979). For a large value of p_0/A_0 satisfying inequality (84), the interface is perfectly bonded. By decreasing p_0/A_0 successively, the slip zone (α_2,β_2) near $\eta=\pi/2$ first appears. Then the slip zone (α_1,β_1) near $\eta=-\pi/2$ occurs when the condition $-1<\Theta^-<0$ holds. With p_0/A_0 approaching $(f\beta)^{-1}\tau_0/B_0$, the stick zone becomes smaller and smaller and disappears at last. The two slip zones (α_1,β_1) and (α_2,β_2), then connect with each other. What will happen once p_0/A_0 drops to the level of $(f\beta)^{-1}\tau_0/B_0$? We will answer this question afterwards.

An interesting phenomenon is observed for $\tau_0=0$. When p_0/A_0 is between 1.1 and 2.9, there is a slip zone near $\eta=-\pi/2$. As p_0/A_0 drops to 1.1, this slip zone disappears until $p_0/A_0=0.2$. After

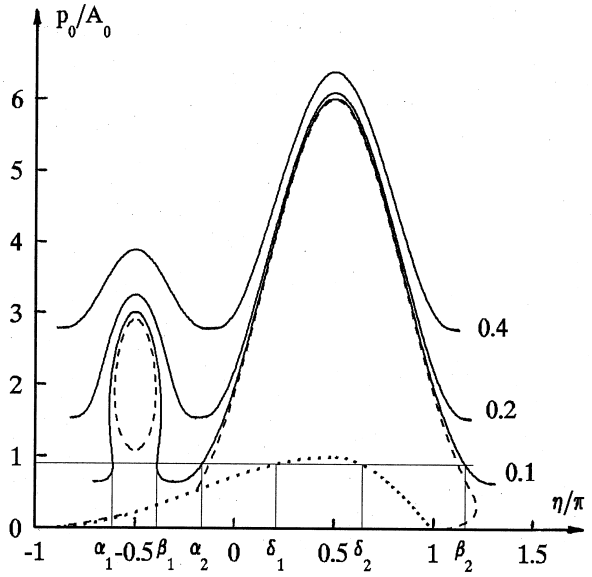

Fig. 4. Extent and location of slip zones for p_0/A_0 and some selected values of τ_0/B_0 with $f\beta = 0.2$, $\theta_0 = 30^\circ$.

that it appears again with a very small area connecting with the trailing edge of the separation zone. No slip zone is found behind the separation zone when $0.2 < p_0/A_0 < 0.5$.

Figure 5 shows the results for $f\beta = 1$, where there is no slip zone near $\eta = -\pi/2$. For smaller values of τ_0/B_0, no slip takes place behind the separation zone when p_0/A_0 is below a certain value. Comparing Figs 4 and 5, one may find that bigger values of τ_0/B_0 and/or smaller values of $f\beta$ will make the interface slip more easily. The influence of the parameter $f\beta$ on the local slip is shown in

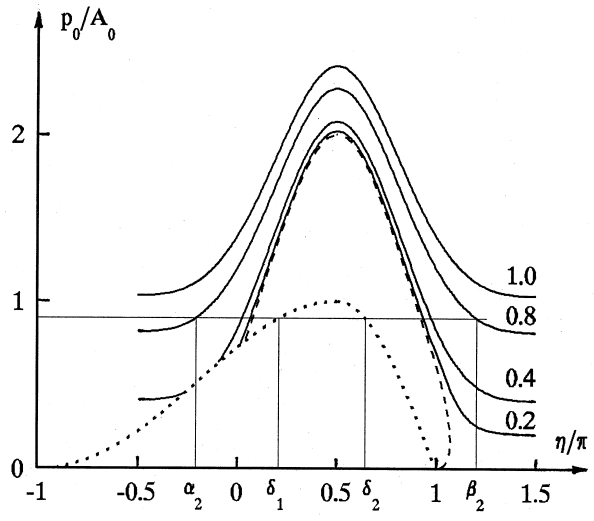

Fig. 5. Extent and location of slip zones for p_0/A_0 and some selected values of τ_0/B_0 with $f\beta = 1$, $\theta_0 = 30^\circ$.

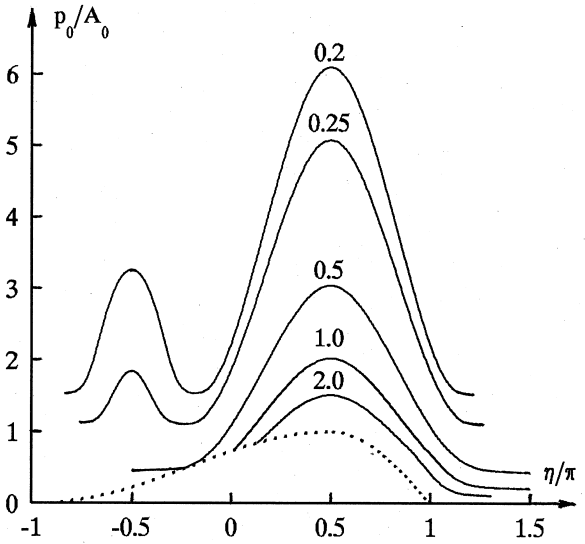

Fig. 6. Extent and location of slip zones for p_0/A_0 and some selected values of $f\beta$ with $\tau_0/B_0 = 0.2$, $\theta_0 = 30^\circ$.

Fig. 6 in detail for $\tau_0/\beta_0 = 0.2$ and $\theta_0 = 30^\circ$. There is a slip zone near $\eta = -\pi/2$ for smaller values of $f\beta$. With $f\beta$ decreasing, the local slip zones become smaller and smaller until all slip zones behind the separation zone disappear.

Figure 7 demonstrates the effects of the parameter α on the local slip of the interface for $\tau_0/B_0 = 0.4$ and $f\beta = 0.2$. The solid, dotted and dashed lines are, respectively, for $\alpha = 1.5$, 2.31845

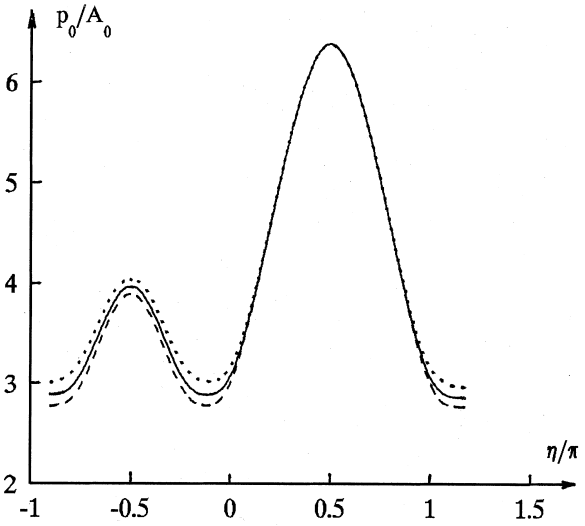

Fig. 7. Effect of parameter α on the extent and location slip zones, $\tau_0/B_0 = 0.4, f\beta = 0.2$.

and 1.07336 (or equivalently for $\theta_0 = 60$, 75 and 30° when the Poisson ratio $v = 0.25$). Only slight differences between lines are observed.

The normalized global sliding velocities, U_1 and U_3, are plotted against p_0/A_0 in Fig. 8 for different values of τ_0/B_0 with $f\beta = 0.2$ and $\theta_0 = 30°$. The dashed line gives the results for $\tau_0 = 0$. The effects of the parameter $f\beta$ are shown in Fig. 9 for $\tau_0/B_0 = 0.4$ and $\theta_0 = 30°$. The dashed lines correspond to $f\beta \to \infty$. In this case the local slip cannot take place, and the solids move just like a worm creeps. It is shown in Figs 8 and 9 that U_3 increases rapidly to infinity, while U_1 to a finite value as p_0/A_0 approaches $(f\beta)^{-1}\tau_0/B_0$. Indeed, one may find the solution in this limiting situation. The relative slip velocities in the separation zones are given by eqn (76). Equation (48) yields

$$\bar{V}_3(\eta) = \bar{U}_3 + \alpha^{-1} f\beta \sin\eta, \quad \bar{V}_1 = \bar{U}_1 + \sin\eta \tag{89}$$

in the slip zones. Considering eqn (74), one can verify that the velocities given by eqns (83) and (96) satisfy eqn (51). Equation (49) requires

$$\bar{U}_3 = \frac{1}{2\pi}\int_{-\pi}^{\pi} \bar{V}_3(\eta)\,\mathrm{d}\eta = \infty, \tag{90}$$

that is, the collapse slipping happens in this case. Unlike in Part I, $\bar{V}_3(\eta)$ in the present case, though infinitely large, is not a constant due to the nonhomogenous distribution of normal traction along the interface. The global sliding velocity in the x_1-direction, U_1, cannot be calculated directly. It should be derived by a limiting procedure. The interface can not transfer in-plane shear motion any more in this limiting case because the in-plane shearing traction on the interface vanishes. However, the normal motion can be transmitted across the interface.

Figure 10 illustrates the distribution of the interface traction, gaps, relative slip velocities in one representative period $(-\pi, \pi)$ for $\tau_0/B_0 = 0.1$, $f\beta = 0.2$, $\theta_0 = 30°$. The dotted, solid, dashed and dot–dashed lines are, respectively, for $p_0/A_0 = 0.6$, 0.9, 2.0 and 3.5. Discontinuities in the interface traction and the relative slip velocities are observed at the trailing edge of the separation zone. The curves are continuous but not smooth at the leading edge. For smaller values of p_0/A_0, a slip zone appears near $\eta = -\pi/2$. This slip zone is relatively small and the slip velocities therein in the x_1-direction are negative (see the dotted, solid and dashed lines). With p_0/A_0 decreasing, the slip and separation zones becomes larger until the two slip zones connect with each other so that there is no stick zone at the interface (see the dotted lines). All quantities except $S_1(\eta)$ increase with p_0/A_0 decreasing. As p_0/A_0 approaches $(f\beta)^{-1}\tau_0/B_0$, $S_1(\eta)$ becomes smaller and smaller and finally vanishes as we have indicated before. It is noted that solid, dashed, dot–dashed lines correspond, respectively, to the cases (j), (b) and (a) shown in Fig. 3.

We next discuss the energy dissipation and partition at the interface. For the particular example considered in this section, a straightforward calculation yields

$$P_1^{\mathrm{PSV}} = \frac{\mu}{4\pi c_{\mathrm{L}}\lambda_2}\left\{\int_{-\pi}^{\pi} V_2^2(\eta)\,\mathrm{d}\eta - \int_{-\pi}^{\pi} [U_1 - V_1(\eta)]V_1(\eta)\,\mathrm{d}\eta\right\}, \tag{91}$$

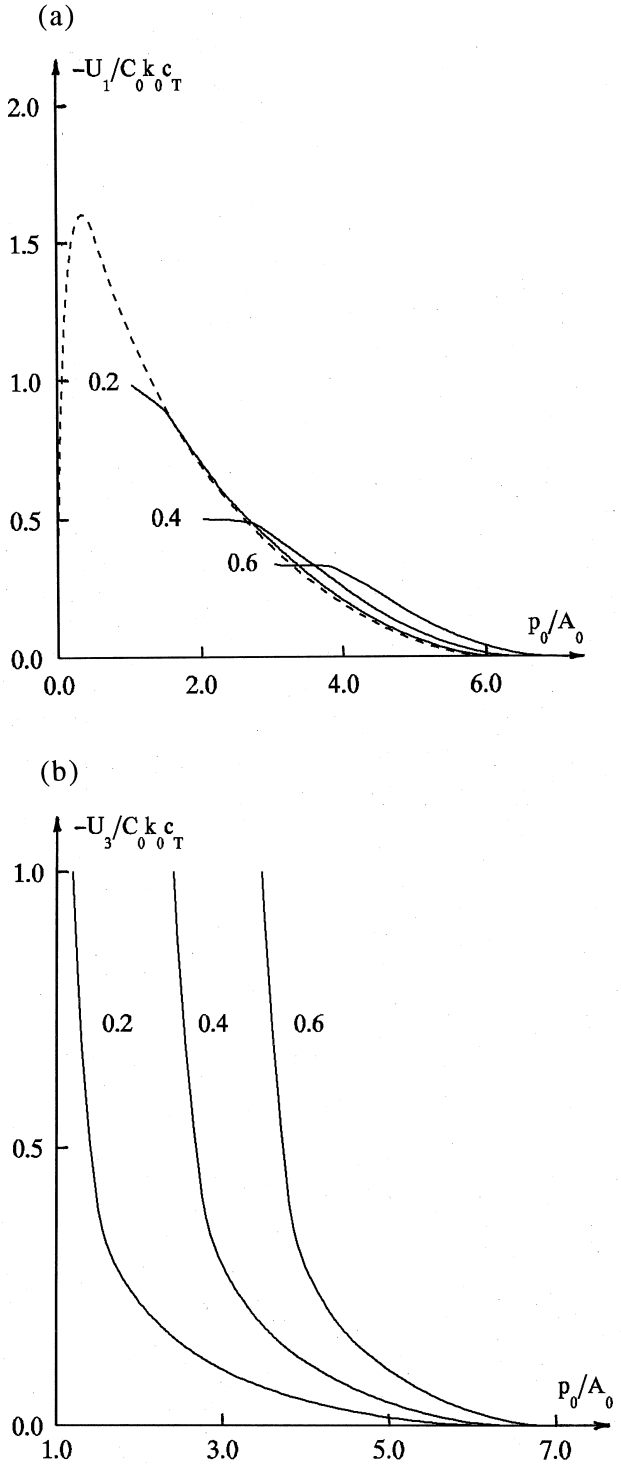

Fig. 8. Dependence of the global sliding (creep) velocities on p_0/A_0 for some selected values of τ_0/B_0 with $f\beta = 0.2$, $\theta_0 = 30^\circ$.

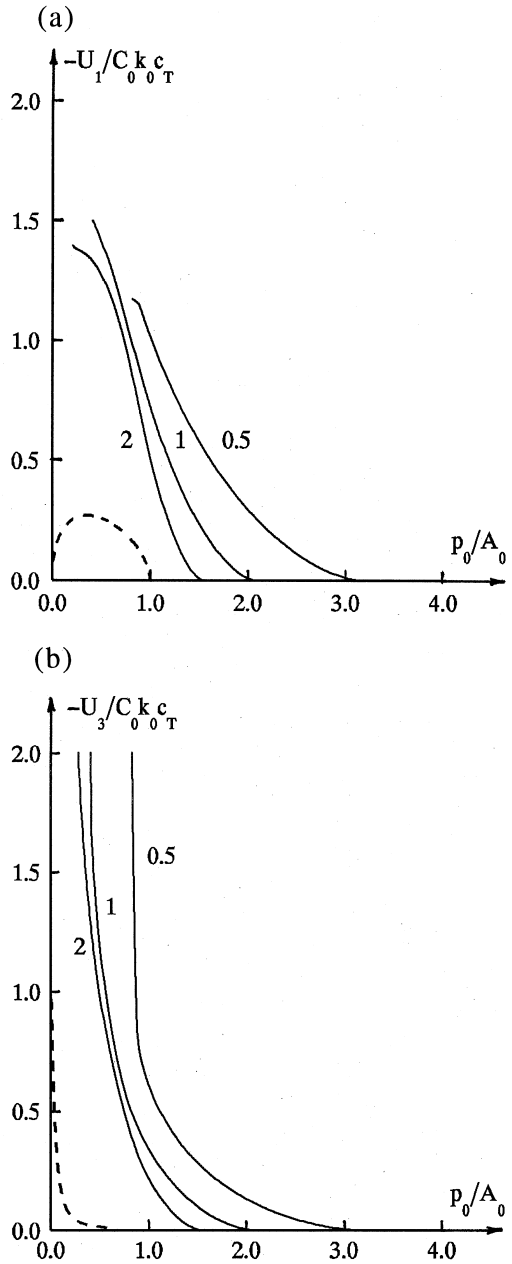

Fig. 9. Dependence of the global sliding (creep) velocities on p_0/A_0 for some selected values of $f\beta$ with $\tau_0/B_0 = 0.4$, $\theta_0 = 30^\circ$.

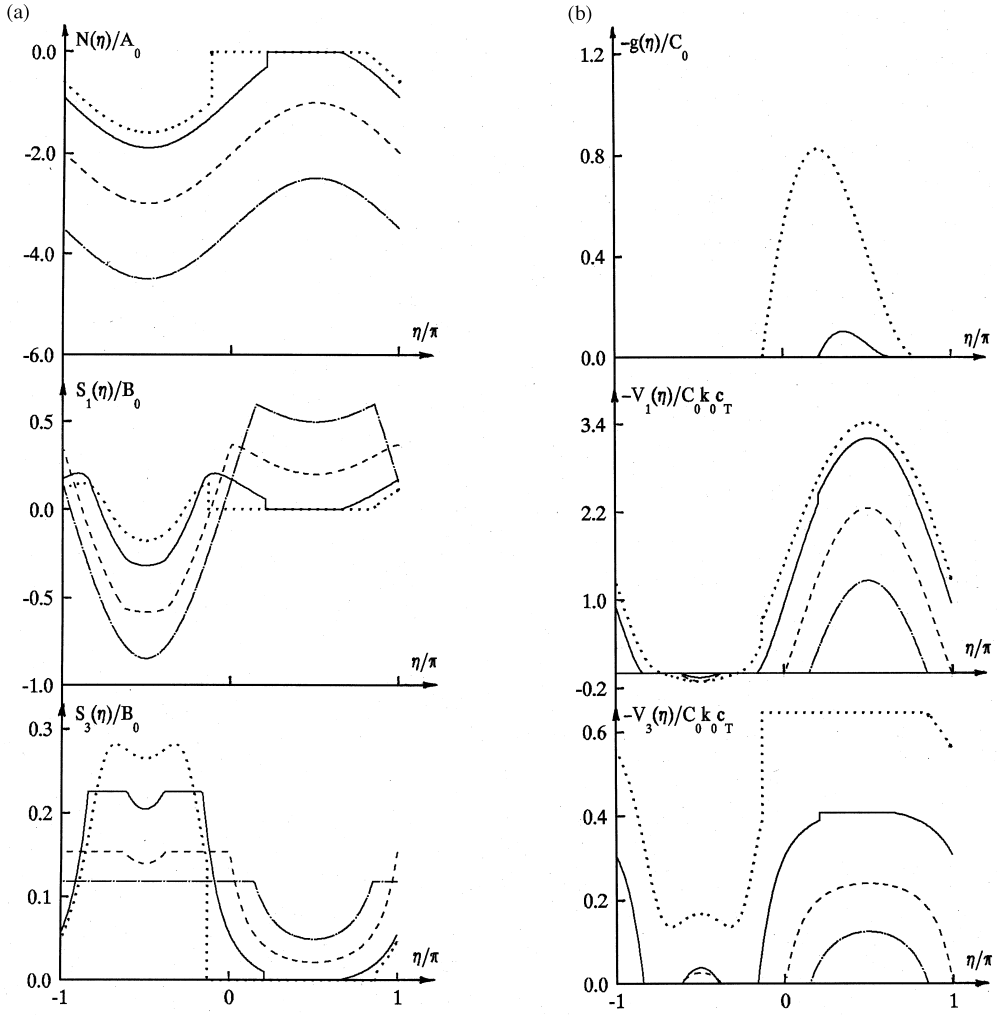

Fig. 10. Distributions of interface traction (a), gaps and relative slip velocities (b) for different values of p_0/A_0 with $\tau_0/B_0 = 0.1, f\beta = 0.2, \theta_0 = 30^\circ$.

$$P_2^{\mathrm{PSV}} = -\frac{1}{2\pi}\int_{-\pi}^{\pi}\left[A_0\sin\eta - \frac{\mu}{c_{\mathrm{L}}\lambda_2}V_2(\eta)\right]\left[C_0 k_{\mathrm{L}} c_{\mathrm{L}}\cos\theta_0\sin\eta - \frac{V_2(\eta)}{2}\right]\mathrm{d}\eta$$
$$-\frac{1}{2\pi}\int_{-\pi}^{\pi}\left\{B_0\sin\eta + \frac{\mu}{c_{\mathrm{L}}\lambda_3}[U_1 - V_1(\eta)]\right\}\left[C_0 k_{\mathrm{L}} c_{\mathrm{L}}\sin\theta_0\sin\eta - \frac{V_1(\eta)}{2}\right]\mathrm{d}\eta, \tag{92}$$

$$P_{\mathrm{d1}} = \frac{1}{2\pi}\int_{-\pi}^{\pi}\left\{B_0\sin\eta + \frac{\mu}{c_{\mathrm{L}}\lambda_3}[U_1 - V_1(\eta)]\right\}V_1(\eta)\,\mathrm{d}\eta, \tag{93}$$

$$P_1^{SH} = P_2^{SH} = -\frac{\mu \cos\theta_2}{8\pi c_T}\int_{-\pi}^{\pi}[U_3 - V_3(\eta)]V_3(\eta)\,d\eta, \tag{94}$$

$$P_{d3} = \frac{1}{2\pi}\int_{-\pi}^{\pi}\left\{\tau_0 + \frac{\mu \cos\theta_2}{2c_T}[U_3 - V_3(\eta)]\right\}V_3(\eta)\,d\eta. \tag{95}$$

It can be verified that

$$P_\tau = P_1^{SH} + P_2^{SH} + P_{d3}. \tag{96}$$

Consequently, we have

$$P_0 = P_1^{PSV} + P_2^{PSV} + P_{d1}. \tag{97}$$

That is to say, part of the energy supplied by τ_0 is partitioned equally over the induced reflected and refracted anti-plane waves, the rest is dissipated due to the frictional slip in the x_3-direction. The energy input of the incident wave is partially extracted by the reflected and refracted in-plane waves, and partially absorbed by friction due to the slip in the x_1-direction.

The power ratios $\{(P_1^{PSV} + P_2^{PSV})/P_0,\ P_{d1}/P_0,\ P_\tau/P_0,\ (P_1^{SH} + P_2^{SH})/P_0,\ P_{d3}/P_0\}$ are plotted vs p_0/A_0 in Fig. 11 for $\tau_0/B_0 = 0.2$ and in Fig. 12 for $\tau_0/B_0 = 0.1$ with other parameters being $f\beta = 0.2$ and $\theta_0 = 30^\circ$. The results for reflected (P_1^{PSV}/P_0) and the refracted (P_2^{PSV}/P_0) in-plane waves are also shown by dashed lines. The power extracted by the induced waves is very small. Most of the power supplied by τ_0 is absorbed by friction. As $p_0/A_0 \to (f\beta)^{-1}\tau_0$, both P_τ and P_{d3} become infinitely large, and the power carried by the induced waves $(P_1^{SH} + P_2^{SH})$ reaches a peak value. Therefore the induced waves are the strongest when catastrophic slip takes place. Also in this limiting situation, most of the power input of the incident wave is extracted by the reflected and refracted in-plane waves. The dissipated power P_{d1} is very small but not zero. All these facts are quite different from those for SH-wave incidence (Wang et al., 1998). It is worth noticing that, when the interface begins to separate, the power extracted by the reflected in-plane waves increases rapidly and that extracted by the refracted waves decreases rapidly (see Fig. 12a). This is understood by considering that the newly-generated free surface reflects the waves totally. For the case of no separation most power input is transmitted across the interface. Turns on the curves are observed at the points indicated by triangles in the figures. These points correspond to the moment when the stick zones disappear.

6. Concluding remarks

In this two-part paper, we examine the re-polarization of elastic waves at a frictional contact interface between two elastic solids loaded by both in-plane and anti-plane shearing traction. For the case of SH wave incidence which involves no separation, the in-plane waves are induced due to the local slip of the interface. For P or SV wave incidence, the anti-plane waves are induced by the local slip with possible separation which is uncoupled with anti-plane motion. The problem is formulated in a general sense. A method to obtain final results is suggested. Special examples for identical material are computed and discussed in detail. The results show that the induced waves have significant effects on the local slip although they only carry a small part of the energy input.

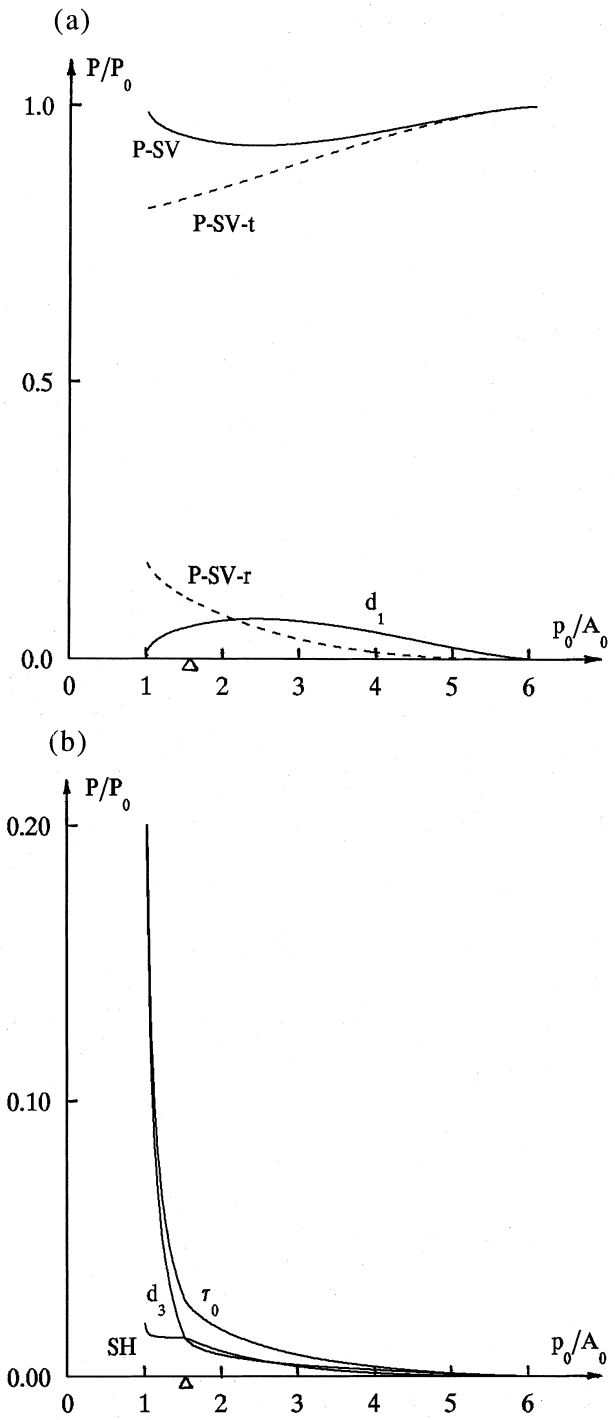

Fig. 11. Energy partition and dissipation for $\tau_0/B_0 = 0.2$, $f\beta = 0.2$, $\theta_0 = 30^\circ$.

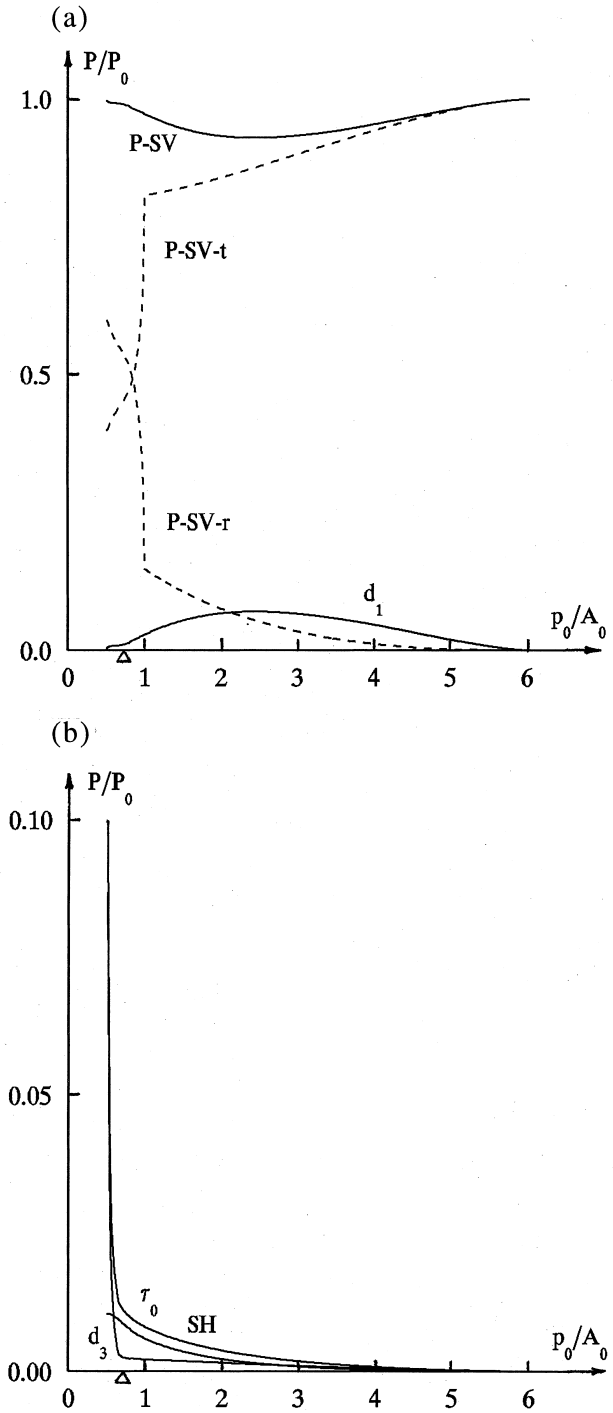

Fig. 12. Energy partition and dissipation for $\tau_0/B_0 = 0.1$, $f\beta = 0.2$, $\theta_0 = 30^\circ$.

The Coulomb friction model is adopted in this series paper. However, the method can be applied in situations involving other nonlinear friction models such as Loeb friction (Loeb, 1961), Förtsch friction (Förtsch, 1956), etc. The paper does not consider the case of super-critical angle incidence. In this situation, one may find that the problem can be cast to a set of nonlinear integral equations which are quite difficult to solve (cf Comninou and Dundurs, 1978 and Comninou et al., 1979 for the cases without re-polarization).

We argue that the re-polarization is a common phenomenon in interaction between elastic waves and a frictional contact interface. As we have known, a wave propagating in a linear homogenous isotropic medium can be generally represented as superposition of P, SV and SH waves. When the boundary conditions are linear, these three types of waves can be treated separately. But for the frictional interface considered here, the three waves are coupled with each other. They are all re-polarized at the interface when local slip takes place. Because the 'apparent velocities' associated with the three waves are different, we cannot solve the problem in the moving coordinate system as we have done in the present paper. The problem is still open and needs to be explored.

Acknowledgement

Support by the China National Natural Science Foundation under Grant No. 19472026 is gratefully acknowledged.

References

Achenbach, J.D., 1973. Wave Propagation in Elastic Solids. North Holland, Amsterdam.

Comninou, M., Dundurs, J., 1977. Reflexion and refraction of elastic waves in presence of separation. Proceedings of the Royal Society of London Series A 356, 509–528.

Comninou, M., Dundurs, J., 1978. Singular reflection and refraction of elastic waves due to separation. Journal of Applied Mechanics 45, 548–552.

Comninou, M., Dundurs, J., 1979. Interaction of elastic waves with a unilateral interface. Proceedings of the Royal Society of London Series A 368, 141–154.

Comninou, M., Dundurs, J., Chez, E.L., 1979. Total reflection of SH waves in presence of slip and friction. Journal of Acoustic Society of America 66, 789–793.

Förtsch, O., 1956. Die ursachen der absorption elasticher wellen. Ann. Geof. 9, 469–524.

Kern, G.A., Kern, T.M., 1974. Handbook of Mathematics. McGraw-Hill, New York.

Loeb, J., 1961. Attenuation des ondes sismiques dans les solids. Geophysics Prospects 9, 370–381.

Wang, Y.-S., Yu, G.-L., Gai, B.Z., 1998. Re-polarization of elastic waves at a frictional contact interface—I. Incidence of an SH wave. International Journal of Solids and Structures 35, 2001–2021.